ORIGINAL PAPER

CrossMark

Aminated polyacrylonitrile nanofibers with immobilized gold-silver core-shell nanoparticles for use in a colorimetric test strip for copper(II)

Mohammed Awad Abedalwafa [1,2] · Yan Li [1] · De Li [1] · Noor Sanbhal [1,3] · Jianmao Yang [4] · Lu Wang [1]

Abstract

The authors describe colorimetric test strips by using electrospun nanofiber membranes (NFMs) carrying gold/silver core/shell nanoparticles (Au/Ag NPs). The Au/Ag NPs were immobilized on aminated porous polyacrylonitrile NFMs to obtain test strips with a tortuous porous structure and a large surface area (38.6 $m^2 g^{-1}$). The color of the resultant NFMs, measured at a wavelength of 420 nm, is red-shifted when exposed to copper ions (Cu^{2+}) with a color change from yellow to pink to colorless. The effect is due to leaching Au/Ag NPs from the NFMs in the presence of ammonium chloride, thiosulfate and Cu^{2+} upon which soluble thiosulfate complexes of Ag^+, Au^{3+} and Cu^{2+} are formed. The effect can be readily seen with bare eyes. Under optimized conditions, this method has a low limit of detection (50 nM at $S/N = 3$), a fast assay time (3 min), good specificity, and excellent reversibility. The colorimetric test strip was successfully applied to the analysis of Cu^{2+} in drinking water sample.

Introduction

Copper serves as a vital cofactor for a variety of enzymes [1]. However, the redox properties of copper ions (Cu^{2+}) would damage the biological system due to its ability to generate reactive oxygen species at an elevated concentration [2]. Currently, the toxicity of Cu^{2+} has been proved, and the

✉ Yan Li
yanli@dhu.edu.cn

✉ Lu Wang
wanglu@dhu.edu.cn

1   Key Laboratory of Textile Science and Technology, Ministry of Education, College of Textiles, Donghua University, Shanghai 201620, China

2   Department of Technical Textile, Faculty of Industries Engineering and Technology, University of Gezira, 21111 Wad Madani, Sudan

3   Department of Textile Engineering, Mehran University of Engineering and Technology, Jamshoro, Sindh 76062, Pakistan

4   Research Center for Analysis and Measurement, Donghua University, Shanghai 201620, China

accumulation of excessive Cu^{2+} can lead to the disturbance of the cellular homeostasis to cause serious neurodegenerative diseases like Menkes, Wilson's, Alzheimer's disease [3]. The routes of Cu^{2+} into the human body are mainly propagated through the food chain with the water media. Therefore, the relevant departments have paid considerable attention to the copper pollution in water. The United States Environmental Protection Agency (EPA) set two kinds of Cu^{2+} concentration limits, 200 nM (acute) and 138 nM (chronic), respectively [4]. Hence, the monitoring of Cu^{2+} in water is of great consequence to us.

Various approaches have been developed for Cu^{2+} determination, such as inductively coupled plasma mass spectrometry [5, 6], atomic absorption spectroscopy [7, 8], atomic emission spectrometry [9, 10] and optical methods [11]. Among these approaches, the optical approach as the prime alternative in analysis assaying area has attracted considerable interest due to their excellent advantages of operational simplicity, reliability, and cost-effectiveness [12–14]. In this case, the colorimetric method consists of the recognition element and transducer, which designed to achieve an assaying process with easy usability, instrument-free, and bare eye detectable signals, seem more convenient. Plenty of Cu^{2+} colorimetric methods [15, 16] have been achieved by selecting rhodamine, coumarin, quinoline, calixarene, noble metal particles (NPs) [17], etc.

as a recognition element. Among them, noble metal NPs are widely concerned because of its distinct physical/chemical attributes, extremely high extinction coefficients, and great surface modifiability [18]. Although colorimetric analytical method based on the noble metal colloid solution, like Au [17, 19–22] and Ag [18, 23] have been achieved, almost all the analytical assay methods were depended on interparticle distance (dispersion or aggregation) optical property. However, the noble NPs colloid solutions also face the problem of susceptible to aggregation by temperature, pH value, or light, lack of portability. Moreover, they also showed insufficient sensitivity due to dilute operation. In addressing these problems, researchers tried to immobilize noble NPs on the filter paper [24], the sensitivity still not adequate due to the large pore size and small specific surface area (SSA). Moreover, the immobilizing NPs amounts are not stable because of lack of specific binding force between filter paper and NPs. All factors have impeded the practical application of existing analytical assay methods in households.

Electrospinning has steadily garnered popularity predominantly due to the promising applications of electrospun nanofibrous membranes (NFMs) in nanoscience [22]. The three-dimensional (3D) structure fibrous membranes can be assembled by the nanofibers with controllable pore structure and SSA. Also, their interconnected tortuous pore structures, which facilitate analyte diffusion and enhance interaction between the analyte with recognition sites [25]. Thus, we assumed that such strips allow for quantitative Cu^{2+} visual detection if assembled by using electrospun NFMs. So far, studies on NFM based Cu^{2+} colorimetric analytical methods have been carried out based on conjugated polymers [26], poly(partic acid) [27], and rhodamine [28]. Benefiting the relatively high SSA, sensitivity has been improved indeed, but the test strips combined noble NPs with NFMs are not available. Consequently, the challenge remains in designing and preparing noble NPs immobilized NFMs with Cu^{2+} visual detection capability and can achieve an EPA satisfactory bare eye limit.

In this study, we present a robust methodology for creating sensitive and selective test strips with the nanofibrous structure using Au/Ag core-shell NPs immobilized aminated polyacrylonitrile (APAN) (Ag/Au@APAN) NFMs. The interparticle distance-dependent color change principle is abandoned, our premise of this design is that the Cu^{2+} has a strong tendency to accelerate Au or Ag NPs' leaching reaction in the sodium hyposulfite ($Na_2S_2O_3$) solution, and the size-dependent optical feature would appear. Herein, the Cu^{2+} detectable NFMs were dexterously fabricated by preparing composite polyvinylpyrrolidone (PVP)/polyacrylonitrile (PAN) precursor nanofibers first; then the nanofibers were extracted with water to remove the PVP, the PAN nanofibers with rough surface were obtained and further modified with ethylenediamine (EDA), as demonstrated in Scheme 1.

Subsequently, Au/Ag core-shell NPs were synthesized and immobilized on the porous PAN NFMs surface via covalent bond [29]. These NFMs achieve integrated assaying performance and rapid response, highly sensitive, excellent selectivity to Cu^{2+}, and rapid response, which can be detected by the naked-eye easily. With its cost-effective design and field portability, these strips can be potentially exploited to determine Cu^{2+}.
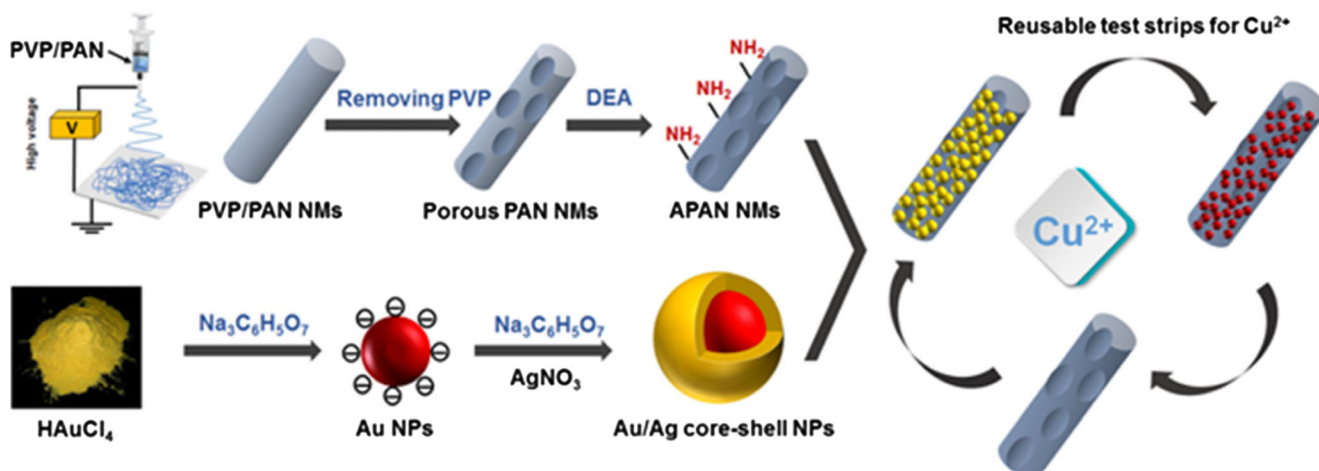
Experimental

All the materials and experimental procedures were presented in the Electronic Supporting Material.

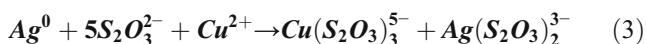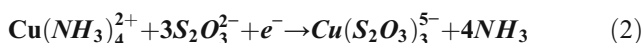## Results and discussion

Assaying principle

Our assaying protocol is inspired by one common used mining technique, which using an ionic system consists of $S_2O_3^{2-}$, NH_4Cl, and Cu^{2+} to leaching silver and gold from ores [30]. Based on these facts, we planned an assumption that if we can immobilize Ag or Au NPs on the substrate without aggregation and then exposure to that ionic system, the size-dependent color changes would happen. In this case, our test strips fabrication pathway mainly should involve three steps: (1) synthesis NPs, (2) fabricating the NFM based substrate, and (3) try to combine them with each other.

Considering the SSA is the key factor for sensitivity, we fabricated the PVP/PAN NFMs first, then removing the PVP component to generate the rough structure, to increase SSA. For NPs, we constructed an Au/Ag core-shell structural nanoparticle, which can produce a richer color change (yellow-pink-white). Furthermore, the aminated NFMs would provide plenty of active sites ($-NH_2$) for NPs immobilizing. These make the test strips available for detecting. During the leaching reaction, the Au/Ag NPs on the NFM surface would immediately form $Ag(S_2O_3)_2^{3-}$ complexes in the presence of dissolved oxygen (Eq.1) depending on the nature of metal-S complexation, and NPs diameters were decreasing happens [31]. When Cu^{2+} exists in the system, it has a strong catalytic effect on the leaching rate of Ag and Au. Cu^{2+} can offset the terroir that a sulfur-like film covered on the NP surface [32]. Subsequently, Cu^{2+} react with NH_4Cl to form $Cu(NH_3)_4^{2+}$ complexes. The $Cu(NH_3)_4^{2+}$ oxidized the Ag or Au in the presence of $S_2O_3^{2-}$ to produce water-soluble $Ag(S_2O_3)_2^{3-}$, $Au(S_2O_3)_2^{3-}$ and $Cu(S_2O_3)_3^{5-}$ (Eq. 2). $Cu(S_2O_3)_3^{5-}$ can be oxidized to $Cu(NH_3)_4^{2+}$ again in the presence of oxygen in solution (Eq. 3). During this process, Cu^{2+} acted as a catalyst and would not be consumed. The leaching rate of Au/Ag NPs increased with the increasing concentration of Cu^{2+}, the size

Scheme 1 Schematic illustration of the experimental procedure, including fabrication of aminated PAN NFMs, synthesized the Au/Ag core-shell NPs and immobilized them on the surface of the NFMs, and detected Cu^{2+} from the impaired water

of the particles was decreased (Fig. S1). As a result, the color of the nanoparticle changes from yellow to colorless.

$$Ag(S_2O_3)_2^{3-} + e^- \rightarrow Ag^0 + 2S_2O_3^{2-} \tag{1}$$

$$Cu(NH_3)_4^{2+} + 3S_2O_3^{2-} + e^- \rightarrow Cu(S_2O_3)_3^{5-} + 4NH_3 \tag{2}$$

$$Ag^0 + 5S_2O_3^{2-} + Cu^{2+} \rightarrow Cu(S_2O_3)_3^{5-} + Ag(S_2O_3)_2^{3-} \tag{3}$$

Characterized Au and Au/Ag NPs structure

Figure 1a and b are demonstrated the transmission electron microscope (TEM) images of Au NPs and Au/Ag core-shell NPs. As for the synthesized colloidal Au NPs, in which Au NPs were dispersed with the spherical shape. After adding $AgNO_3$, the distinct layer of Ag can observe in the TEM image insets Fig. 1b. Moreover, the Au/Ag core-shell NPs also are not aggregated. To further verify the synthesis of Au/Ag core shell NPs is completed, their corresponding UV-via spectra were also identified by strong surface plasmon resonance (SPR) peaks (Fig. 1c). The wine-red colored Au NPs shows an obvious SPR peak at 518 nm, indicating the spherical shaped Au NPs [33] have been prepared. Moreover, Au/Ag core-shell NPs only possess one SPR peak around 395 nm, which indicated the Ag shell [34] have covered on the Au seeds surface. Importantly, after Ag shell growth on to the Au seeds, the peak at 518 nm for Au core disappeared. Considering the intensity of the Au core decreased as the thickness of the Ag shell increased [35], it can be deduced that the Au/Ag NPs structure formed. The particles size distribution of Au NPs and Au/Ag NPs suspension measured by dynamic light scattering (DLS) technique. As shown in Fig. 1d, both samples were displayed in a narrow diameter distribution, indicating that there is no aggregation occurred during the entire growth process. The diameter of Au NPs is 13.7 nm, and the Au/Ag NPs exhibits a diameter of 21.0 nm.

Structural features of PVP/PAN NFMs before and after removing PVP

After the Au/Ag NPs have been successfully prepared, a further investigation was performed to optimize the SSA and porous structure of the NFM based substrate. A series of bi-component PVP/PAN NFMs with different weight ratio (P_1P_3, P_1P_2, P_1P_1, P_2P_1, and P_3P_1) were fabricated. The influences of the composition on the morphology, SSA, and pore size were analyzed. Since our purpose is removing the PVP component to generate the rough structure, the mass loss ratio of PVP ($R_{pvp}\%$) was calculated (Eq. 4) first.

$$R_{PVP} = \frac{w_0 - w_1}{w_0} \times 100\% \tag{4}$$

Where W_0 and W_1 are the mass of P_xP_y and P_xP_y', respectively.

Table S2 lists the mass loss of PVP in the bi-component NFMs before and after water extraction. It was clear that the mass loss ratio showed an increasing trend with the increase of PVP content in bi-component nanofibers, and the mass loss rate was increased from 82 to 92.2%. That may ascribe to the fact that the molecular weight of PVP is higher than PAN in this study, and the most of PVP component would distribute on nanofiber surface. Thus, facilitate the interaction between water with PVP. Furthermore, the mass loss rate cannot reach 100% even the treating time extend to 72 h due to the PVP component inner composite fibers. Thankfully, it only needs 3 min to detect Cu^{2+} at 60 °C; then, the residual PVP would not interfere the Cu^{2+} detection.

On the purpose of constructing a substrate for Au/Ag NPs immobilizing, some criteria should be followed, such as the nanofibrous and porous structure should not be sacrificed and the P_xP_y NFMs must not disintegrate after the water extraction process. Herein, Fig. S2 provides the photograph and the FE-SEM images of P_xP_y NFMs before and after treatment with
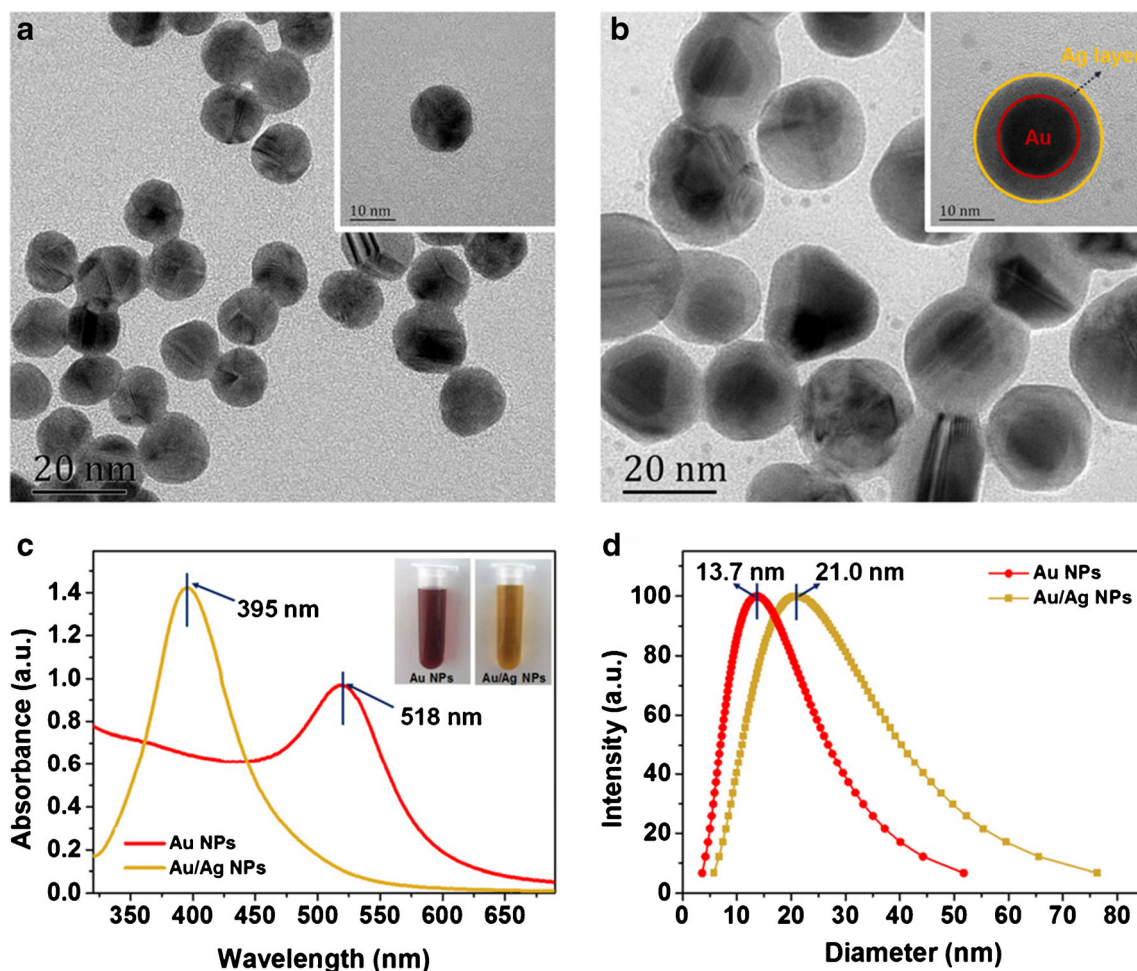
Fig. 1 TEM images of (**a**) Au NPs and (**b**) Au/Ag NPs, their corresponding UV-vis absorption spectra and DSL curves are displayed in (**c**) and (**d**)

water extraction. As shown in Fig. S2a, all the P_xP_y underwent a perceptible shape size shrinkage after water extraction. Especially, the P_2P_1 and P_3P_1 samples, a color change from white to transparent also came together, which makes them no longer viable for further modification. Afterward, some representative FE-SEM images of P_xP_y and $P_xP_y{}'$ were observed and showed in Fig. S2b-d, 2b'-d', and Fig. S3. As for P_1P_3, P_1P_2, P_1P_1, and P_2P_1, some individual nanofibers with smooth surface comprise the mat, and the average diameters of these samples are 279, 365, 392, and 462 nm, respectively, which were increased with the increase of PVP content in the NFMs. By contrast, the conductivity and viscosity as listed in Table S3. With the increasing of PVP component, the conductivities were almost unchanged. That is to say; the fiber diameter increasing may due to the viscosities of the precursor solutions was increased when increasing the content of PVP [36]. In addition, as presented in Fig. S3b, the fibers in the P_3P_1 NFMs have swelled and bonded together; the average diameter increased to 912 nm, which may be because the PVP component tends to distribute on the surface of the fiber and automatically absorb water from the atmospheric environment.

After undergoing 2 h treatment, the nanofibers in $P_1P_3{}'$, $P_1P_2{}'$, and $P_1P_1{}'$ are no longer smooth, some roughness structures have shown. Besides, as for the other two samples with higher PVP content (>50%), the 3D nanofibrous structures of P_2P_1 and P_3P_1 have been destroyed, since the swelling ratio of the NFMs has a direct relationship with PVP content. From the FE-SEM images shown in Fig. S2b', S2C', and S2d', we can also find out that the P_1P_1 with more rough structure than the other two samples. Obviously, the extraction of PVP component has also influent the porous structure of the NFMs, thereby interfere the assaying performance towards Cu^{2+}. The N_2 adsorption-desorption isotherms and the capillary flow porosimetry were recruited here to assess the water extraction induced variation in BET surface areas and porous structures of the relevant NFMs, except for P_2P_1 and P_3P_1 (both are without nanofibrous structure and transparent), the results illustrated in Fig. 2a, b and Table S4. It is worth to note that all the NFMs samples exhibited a typical IV isotherm feature with a palpable H_3 hysteresis loop in a p/p_0 range from 0.5 to 0.9, indicating 2 h water extraction process has not decimated the pristine characteristics of open mesopore [37]. According to the data listed in Table S4, it can be noted that
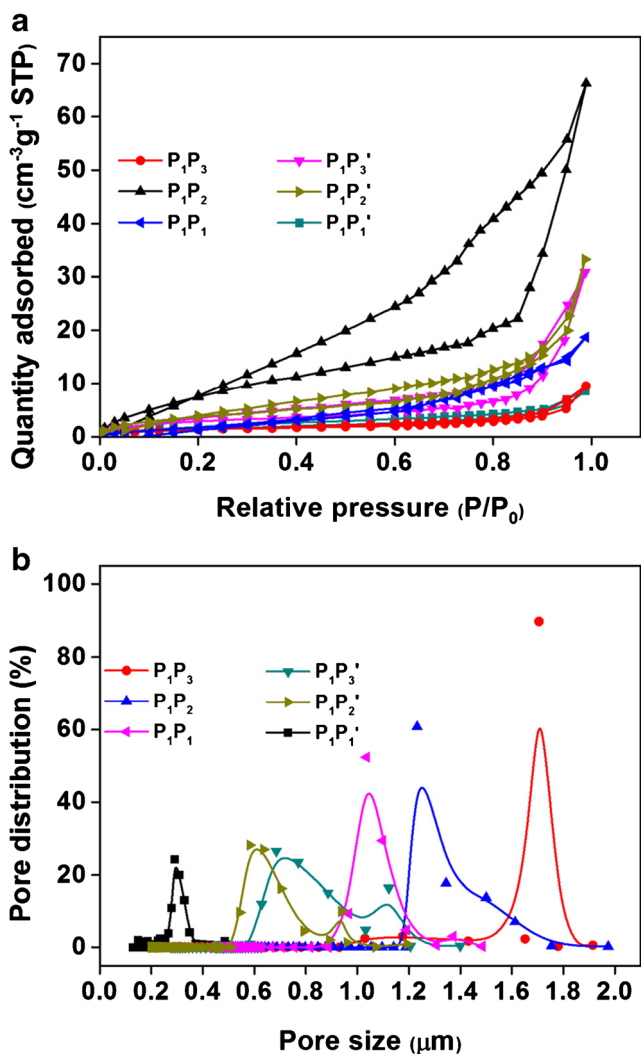
a

b

Fig. 2 **a** N_2 adsorption-desorption isotherms of relevant P_1P_1, P_1P_1', P_1P_2, P_1P_2', P_1P_3, and P_1P_3', their Pore size distribution curves are displayed in **b**

a certain increase of the SSA in the bi-component nanofibers (P_1P_1, P_1P_2, and P_1P_3) which is ascribed to the decrease of the nanofibers diameter. Moreover, the P_1P_1' possesses the highest SSA (38.6 m^2 g^{-1}), and its PVP content is more than the other two samples. That is to say, with the decrease of PVP content in bi-component nanofibers, the SSA decreasing accordingly. The pore size and distribution are shown in Fig. 2b, the P_xP_y displayed unimodal size distribution from 1.06 to 1.71 μm, and the P_xP_y NFMs with more PVP content showing smaller pore size, this is constant with the water absorbing ability of PVP, and the swell ratio increasing would result in smaller pore size. As for P_xP_y', the pore size of samples have shrunk from a few micrometers to nanometers, which can benefit rapid transmission of reagents into nanofibrous networks and enhance the interaction between fibers with Cu^{2+} [38]. Considering the SSA is the key fact for test strips sensitivity, the P_1P_1' sample was selected for the subsequent studies.

Preparing EDA functionalized P_1P_1' for au/ag NPs immobilization

Attempting to provide a substrate for Au/Ag NPs immobilization and provide a certain chemical bond, amination experiment was performed here according to the reaction listed in Fig. S4a. Since the PVP content was already removed from P_1P_1, the name of P_1P_1' was set as PAN and the EDA modified PAN was named as APAN. The graft EDA on porous PAN nanofibers surfaces can be confirmed by FT-IR spectra analysis as shown in Fig. S4b. For PAN sample, the peaks around 2249 cm^{-1} represented the C≡N stretching. Moreover, the peak at 1574 cm^{-1} and 3300~3500 cm^{-1} in PVP sample are N-H bending and stretching, respectively. The APAN sample exhibit a new strong broad-band range from 3300~3500 cm^{-1} that correspond to the overlapping bands of both OH and stretching vibration of N-H groups after amination. A new peak appeared at 1574 cm-1 was the bending vibration band of N-H group, those indicated that the graft of EDA on porous PAN nanofibers. Thus, we deduce that the APAN nanofibers membrane with largest SSA and anime group have been generated successfully. The titration experiments were performed 5 times to obtain the average content of –NH$_2$ according to Eq. 5.

$$A = \frac{C(V_1 - V_0)}{w_0} \tag{5}$$

Where A is the content of –NH$_2$ (mM g^{-1}), C is the concentration of standard solution, V_1 is the volume of HCl solution that APAN NFMs used, V_o is the volume of control sample used HCl solution. The calculated results were listed in Table S5, and the average –NH$_2$ content is 2.69 mM, which is feasible for NPs immobilizing, since increasing the grating amount of the –NH$_2$ content would also induce some obvious changes, the NFMs became brittle, and the color of the NFMs changed from white to yellow [39], which is not suitable as our platform.

The successfully spotting Au/Ag NPs on APAN was confirmed by FE-SEM images as showed in Fig. 3. The average diameter of APAN NFMs had shrunk to 236 nm, and the roughness increased after amination process, which is displayed in Fig. 3a. After spotting the Au/Ag NPs on the APAN, the particle-shaped structure can be observed in Fig. 3b. These particles covered structure is indicating the interaction between Au/Ag NPs and the amino functional groups indeed existed. Therefore, Au/Ag NPs were firmly immobilized on the APAN via two major bonding factors: (a) the anchoring N-Au/Ag bonds and (b) the nonconventional N-H Au/Ag hydrogen bonds [29]. In addition, the size and shape of the particle have no obvious change as we can see from the high magnification FE-SEM image shown Fig. 3b'. It also can be seen that monodisperse Au/Ag core-shell NPs
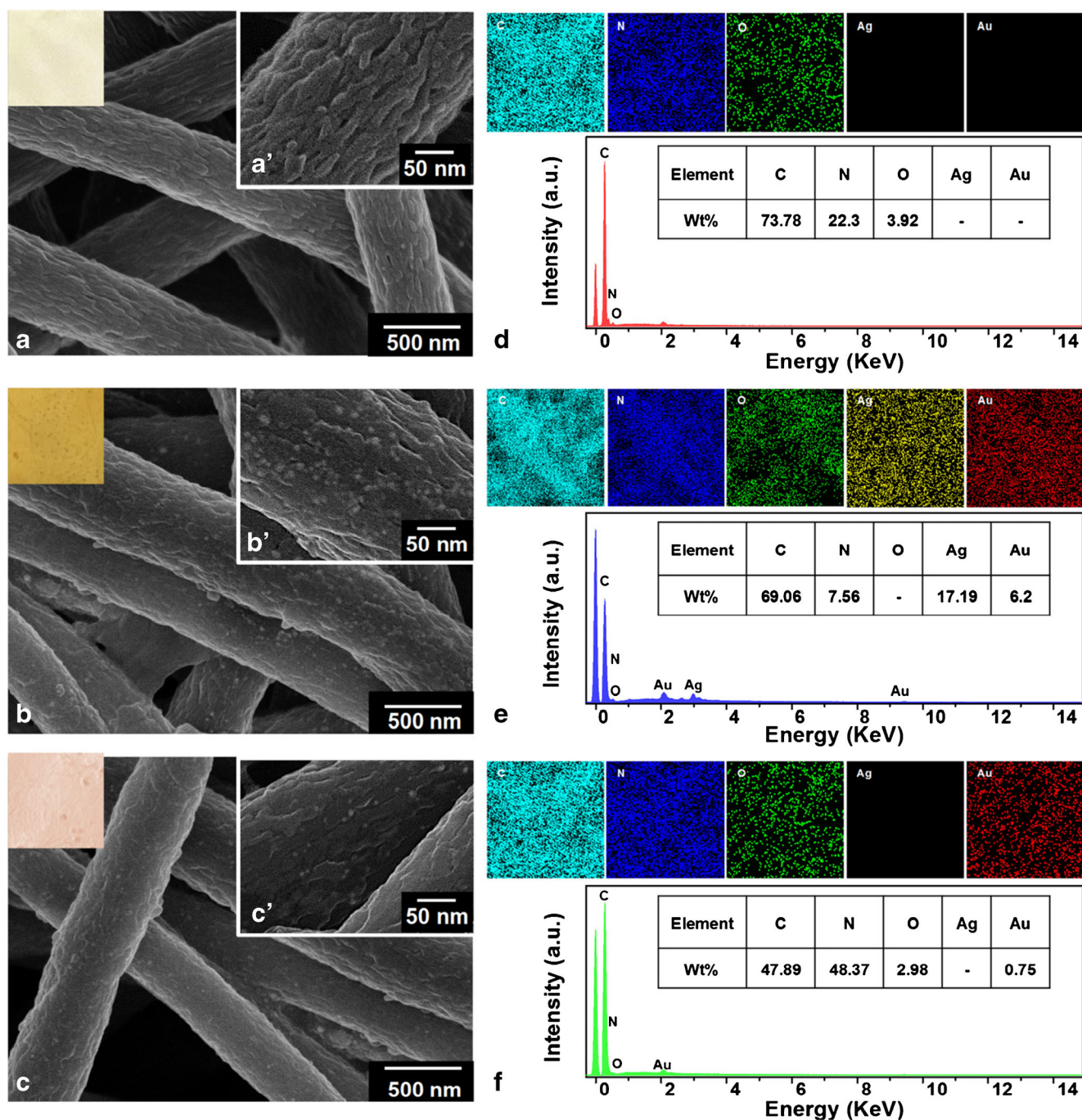
Fig. 3 FE-SEM images of (**a**) APAN, (**b**) Au/Ag NPs probe APAN and (**c**) Au/Ag NPs immobilized APAN NFMs after incubated in the 60 °C leaching liquor with 15.7 μM Cu^{2+} for 3 min; insets show the corresponding optical images. (**a'**) (**b'**), and (**c'**) are the corresponding

images at high magnification. (**d**), (**e**), and (**f**) are the corresponding EDX spectrum, insets show the corresponding elemental mapping and weight ratio

probes were distributed on APAN. After reacting with 15.7 μM Cu^{2+} for 3 min at 60 °C leaching liquor, the color of the strip changes from yellow to pink, which was attributed to the decreased diameter of NPs. The FE-SEM images of 15.7 μM Cu^{2+} assay sample presented the dramatic decrease in coverage scale and diameter of nanoparticles as showed in Fig. 3c, which were in good accordance with the phenomenon

of Au/Ag core-shell NPs immobilized APAN NFMs' color change. Besides that, the amounts of Au/Ag NPs probe have obviously reduced after assaying.

Moreover, energy-dispersive X-ray spectroscopy (EDX) was used to determine the amount of Au and Ag elements in the NFMs, and also the distribution of the Ag/Au NPs in the NFMs was monitored by EDX mapping and represented in

Fig. 3d-f. As can be seen (Fig. 3e), the coexistence of Au and Ag elements demonstrates that the Au/Ag NPs have been immobilized successfully on the NFMs. In contrast, the EDX spectrum of the APAN NFMs before NP loading do not show the signals of Au and Ag (Fig. 2d). In another hand, the EDX spectrum after Cu^{2+} detection does not show the signals of Ag and the weight ratio of Au is reduced (Fig. 3f), which agree with the results mentioned above, that Au/Ag NPs can leach out from the NFMs by using the ionic system.

The loading amount of Au/Ag NPs were increasing with the immersing time's increases. As illustrated in Fig. 4a, from the UV-vis spectra we can find the absorption peak of Au/Ag NPs immobilized APAN (Au/Ag@APAN) NFMs were located at 420 nm, and the intensity tended to be stable when immersing time is above 11. Therefore, the APAN immersing in Au/Ag NPs colloid for 11 times with yellow color shown in Fig. 4b was used as the control sample of the test strips.

Assaying performance analysis and optimization

The feasibility of our protocol has been proved above. However, the sensitivity of the test strips containing the Au/Ag NPs and APAN NFMs for Cu^{2+} detection is related to various factors, including the concentration of NH^{4+}, $S_2O_3^{2-}$, pH of the solution, and the incubation time. Therefore, these parameters were further optimized by using 15.7 μM of Cu^{2+}. The different change of the color of the test strips was

determined by relative absorbance intensity (A_{500nm}/A_{420nm}) using UV-via spectra. Firstly, the influence of the concentration of NH_4Cl was investigated in the concentration range of 10 to 60 mM (Fig. S5a). In our assaying system, NH_4^+ plays a role of Cu^{2+} protector. When NH_4^+ and Cu^{2+} coexisted, the increasing concentration of NH_4^+ would promote the chance of forming $Cu(NH_3)^{2+}$, not precipitate. As a consequence, the further leaching reaction between Cu^{2+} and Au/Ag core-shell NPs would carry on smoothly. The A_{500nm}/A_{420nm} was almost constant above 50 mM in the presence of Cu^{2+}. Therefore, 50 mM of NH_4Cl was selected as the optimal value for all experiments. Furthermore, generally speaking, various factors control the interaction between test strips and Cu^{2+}, for instance, the complex sites functionality, the solubility and the existed species of Cu^{2+}. In this case, the Cu^{2+} colorimetric detection processes were performed at different pH media (pH values from 7 to 12). As shown in Fig. S5b, when the pH value of the solution was 7 and 8, the A_{500nm}/A_{420nm} ratios were relatively small. Considering the solubility product constant of $Cu(OH)_2$ is 2×10^{-19} ($T = 298$ K), the low A_{500nm}/A_{420nm} value may owing to the instability of $S_2O_3^{2-}$ was not stable, it broke down to sulfate, sulfide, sulfite tetrathionate, trithionate, polythionates, and polysulfides [30]. Therefore, increasing the pH may improve the stability of $S_2O_3^{2-}$. The species that Cu^{2+} prefer to stay is $Cu(NH_3)^{2+}$, and the concentration of $Cu(NH_3)^{2+}$ increased with the increase of pH value since the alkaline environment can promote the formation of

Fig. 4 a UV-vis absorption spectra and b optical images of the APAN immersing in Au/Ag NPs colloid solution for different times
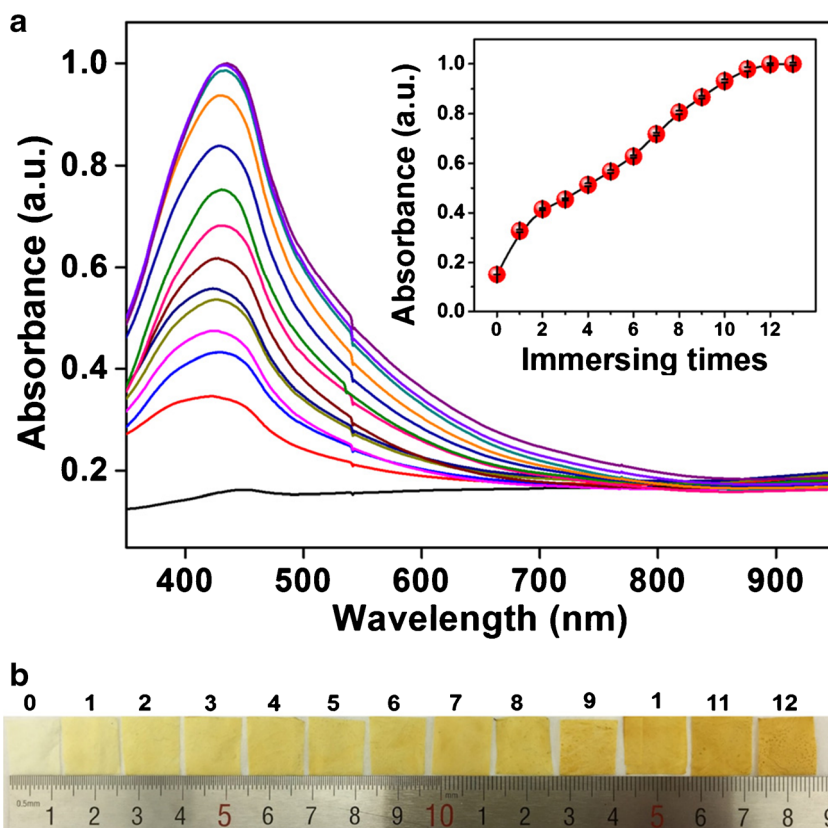
NH_3 from NH_4^+. As a result, the A_{500nm}/A_{420nm} was nearly constant above pH 11 in the presence of 15.7 μM Cu^{2+}. From the facts above we can deduce that the $S_2O_3^{2-}$ also effects the assaying performance, thus the $S_2O_3^{2-}$ concentration was examined in the range of 1.0 to 11.0 mM. As shown in Fig. S5c. The A_{500nm}/A_{420nm} value increased with the increasing of $S_2O_3^{2-}$ concentration and achieved the maximum value at 9 mM of $S_2O_3^{2-}$, which was selected as the optimal concentration. Ultimately, the effect of incubating time with the optimized condition above was also investigated. As shown in Fig. S5d, the A_{500nm}/A_{420nm} value increased with the increasing of incubating time and then became constant in the concentration of 15.7 μM Cu^{2+} after 3 min. Therefore, the A_{500nm}/A_{420nm} was tested within 3 min after the strip immersing into the solution.

The selectivity of the strips was estimated with other sulfate metallic salts such as Li^+, Na^+, K^+, Mg^+, Ca^{2+}, Zn^{2+}, Mn^{2+}, Cd^{2+}, Cr^{3+}, Al^{3+} Co^{2+}, Ni^{2+}, Ag^+, Pb^{2+}, Fe^{3+}, Hg^{2+}, and their Cu^{2+}complex. They were at a concentration of 15.7 μM, after incubating into the optimized leaching liquor (50 mM NH_4Cl, pH 11 and 9.0 mM $Na_2S_2O_3$) for 5 min. As shown in Fig. S6a and b, only Cu^{2+} and their complex can oxidize the Au/Ag NPs, resulting in the color change of the Au/Ag NPs (yellow-pink-colorless), which was visible by the bare eye. This result indicates that this analytical method offers a promising selectivity for the detection of Cu^{2+}.

The sensitivity performance of the colorimetric strips was evaluated by spiking in leaching liquor with various concentrations of Cu^{2+} under the optimized conditions. As shown in Fig. 5a, the relative absorbance intensity of colorimetric strips increased gradually with the increasing of Cu^{2+} concentration, and the absorption peak also exhibited blueshift from 420 nm to 500 nm, indicating that the Cu^{2+} has a catalyst accelerating effect on the leaching of Au/Ag NPs. We also obtained a linear relationship ($R^2 = 0.9916$) between the relative absorbance (A_{500nm}/A_{420nm}) and the concentration of Cu^{2+} in the range from 0.05 to 1 μM, as shown in Fig. 5b. Figure 5c presents the photographs of colorimetric strips for different concentrations of Cu^{2+} ions, revealing an obvious color change from yellow to pink to white by the increasing of Cu^{2+} concentrations. A lower limit of detection (LOD) of 50 nM is obtained, which is lower than another analytical method as shown in Table S6. Besides sensitivity, reusability of the strips is another essential factor, which can prove it has certain environmental friendliness. If test strips react with Cu^{2+}, it would be immersed into the Au/Ag NPs solution again, the yellow color of the sample rapidly appeared again. As illustrated in Fig. S7, the initial absorbance of Au/Ag NPs@APAN at 420 nm was 0.998, upon chromatic reaction, the absorbance decreases to 0.181. By further immersing the test strips with Au/Ag NPs colloid, the absorbance increased to 0.998. Besides the first cycle, it exhibited good reproductively at every repetition and shown a
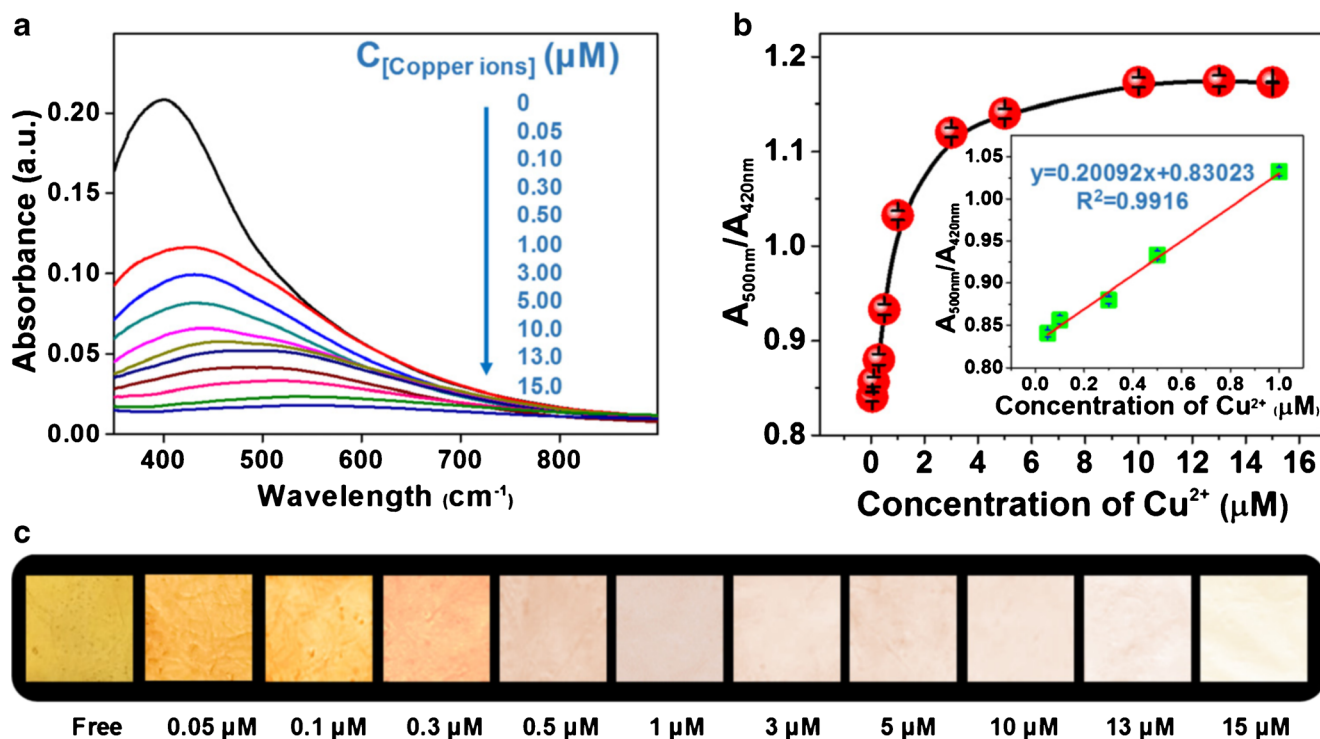

Fig. 5 **a** UV-vis absorption spectra, **b** plot of (A_{500nm}/A_{420nm}) values versus Cu^{2+} concentration, and **c** optical images of the colorimetric strips after colorimetric test in optimized leaching liquor added with different concentrations of Cu^{2+} for 5 min. Inset in (b): the enlarged portion of the plot in the Cu^{2+} concentration range of 0.05~1 μM

slight increase in absorbance after 6 cycles. Even so, the test strips have a certain of reusability.

To evaluate the promising application of the strip, drinking water was spiked with different Cu^{2+} concentrations, since the concentration of Cu^{2+} in drinking water was zero or much lower than the limit of detection of the strip. The concentration determined by the colorimetric strip was found in good agreement with those obtained by ICP-AES. Moreover, the average recoveries were found between 98.26% – 104.52% with the relative standard derivations (RSD) in the range of 0.15% – 0.62% (Table S7). The results indicated the high potential applicability of the test strip for the determination of Cu^{2+} in real samples.

Conclusions

In summary, we have fabricated a colorimetric strip for rapid and real-time detection of copper ions by the Au/Ag NPs immobilized amine porous PAN NFMs. Taking advantages of the fascinating features of the NFMs and the rapid reaction of the catalyst system, the strips possessed a promising selectivity toward other metal ions and a high sensitivity under the optimized liquor system, which is lower than the EPA's standard for copper ions in drinking water. This method avoided the need for sophisticated equipment and professional, providing a quick system for the detection of Cu^{2+} ions. This assaying sets a remarkable example of catalytic leaching in analytical chemistry for the analysis of heavy metal ions by using nanotechnology, which also provided potential applications in the environmental monitoring and biological detection fields.

Compliance with ethical standards The author(s) declare that they have no competing interests.

References

1. Gaetke LM, Chow CK (2003) Copper toxicity, oxidative stress, and antioxidant nutrients. Toxicology 189(1):147–163. https://doi.org/10.1016/S0300-483X(03)00159-8

2. Wang J, Sheng Li R, Zhi Zhang H, Wang N, Zhang Z, Huang CZ (2017) Highly fluorescent carbon dots as selective and visual probes for sensing copper ions in living cells via an electron transfer process. Biosens Bioelectron 97:157–163. https://doi.org/10.1016/j.bios.2017.05.035

3. Kim Y-R, Kim HJ, Kim JS, Kim H (2008) Rhodamine-based "turn-on" fluorescent Chemodosimeter for cu(II) on ultrathin platinum films as molecular switches. Adv Mater 20(23):4428–4432. https://doi.org/10.1002/adma.200801001

4. Cruz L, Roberts C, Reiley M, Santore R, Paquin P, Chapman G, Mitchell J, Delos C, Meyer J, Mathew R (2007) Aquatic life ambient freshwater quality criteria-Copper. Washington DC: United States Environmental Protection Agency. Office of Water, Office of Science and Technology. EPA-822-R-07-001. https://www.epa.gov/wqc/aquatic-life-criteria-copper

5. Becker JS, Matusch A, Depboylu C, Dobrowolska J, Zoriy MV (2007) Quantitative imaging of selenium, copper, and zinc in thin sections of biological tissues (slugs−genus Arion) measured by laser ablation inductively coupled plasma mass spectrometry. Anal Chem 79(16):6074–6080. https://doi.org/10.1021/ac0700528

6. Konz T, Migliavacca E, Dayon L, Bowman G, Oikonomidi A, Popp J, Rezzi S (2017) ICP-MS/MS-based Ionomics: a validated methodology to investigate the biological variability of the human Ionome. J Proteome Res 16(5):2080–2090. https://doi.org/10.1021/acs.jproteome.7b00055

7. Baytak S, Kasumov VT (2017) Preconcentration and determination of copper(II) by novel solid-phase extraction and high-resolution continuum source flame atomic absorption spectrometry. Anal Lett 50(1):105–116. https://doi.org/10.1080/00032719.2016.1170136

8. Ajtony Z, Laczai N, Dravecz G, Szoboszlai N, Marosi Á, Marlok B, Streli C, Bencs L (2016) Fast and direct screening of copper in micro-volumes of distilled alcoholic beverages by high-resolution continuum source graphite furnace atomic absorption spectrometry. Food Chem 213:799–805. https://doi.org/10.1016/j.foodchem.2016.06.090

9. Yu J, Yang S, Lu Q, Sun D, Zheng J, Zhang X, Wang X, Yang W (2017) Evaluation of liquid cathode glow discharge-atomic emission spectrometry for determination of copper and lead in ores samples. Talanta 164:216–221. https://doi.org/10.1016/j.talanta.2016.11.015

10. Lu Q, Yang S, Sun D, Zheng J, Li Y, Yu J, Su M (2016) Direct determination of cu by liquid cathode glow discharge-atomic emission spectrometry. Spectrochim Acta B At Spectrosc 125:136–139. https://doi.org/10.1016/j.sab.2016.09.019

11. Hu Y, Zhang J, Lv Y-Z, Huang X-H, Hu S-l (2016) A new rhodamine-based colorimetric chemosensor for naked-eye detection of Cu2+ in aqueous solution. Spectrochim Acta A Mol Biomol Spectrosc 157:164–169. https://doi.org/10.1016/j.saa.2015.12.031

12. Huang L, Chen K, Zhang W, Zhu W, Liu X, Wang J, Wang R, Hu N, Suo Y, Wang J (2018) ssDNA-tailorable oxidase-mimicking activity of spinel MnCo2O4 for sensitive biomolecular detection in food sample. Sensors Actuators B Chem 269:79–87. https://doi.org/10.1016/j.snb.2018.04.150

13. Huang L, Zhu W, Zhang W, Chen K, Wang J, Wang R, Yang Q, Hu N, Suo Y, Wang J (2017) Layered vanadium(IV) disulfide nanosheets as a peroxidase-like nanozyme for colorimetric detection of glucose. Microchim Acta 185(1):7. https://doi.org/10.1007/s00604-017-2552-1

14. Liu X, Zhang W, Huang L, Hu N, Liu W, Liu Y, Li S, Yang C, Suo Y, Wang J (2018) Fluorometric determination of dopamine by using molybdenum disulfide quantum dots. Microchim Acta 185(4):234. https://doi.org/10.1007/s00604-018-2771-0

15. Wen R, Li H, Chen B, Wang L (2017) Facile preparation of fluorescent gold nanocluster via polysaccharide-templated approach and its application for Cu2+ sensing. Sensors Actuators B Chem 248:63–70. https://doi.org/10.1016/j.snb.2017.03.130

16. Udhayakumari D, Naha S, Velmathi S (2017) Colorimetric and fluorescent chemosensors for Cu2+. A comprehensive review from the years 2013-15. Anal Methods 9(4):552–578. https://doi.org/10.1039/C6AY02416E

17. Liu R, Chen Z, Wang S, Qu C, Chen L, Wang Z (2013) Colorimetric sensing of copper(II) based on catalytic etching of gold nanoparticles. Talanta 112:37–42. https://doi.org/10.1016/j.talanta.2013.01.065

18. Oliveira E, Núñez C, Santos HM, Fernández-Lodeiro J, Fernández-Lodeiro A, Capelo JL, Lodeiro C (2015) Revisiting the use of gold and silver functionalised nanoparticles as colorimetric and fluorometric chemosensors for metal ions. Sensors Actuators B Chem 212:297–328. https://doi.org/10.1016/j.snb.2015.02.026

19. Weng Z, Wang H, Vongsvivut J, Li R, Glushenkov AM, He J, Chen Y, Barrow CJ, Yang W (2013) Self-assembly of core-satellite gold nanoparticles for colorimetric detection of copper ions. Anal Chim Acta 803:128–134. https://doi.org/10.1016/j.aca.2013.09.036

20. Yang J, Zhang Y, Zhang L, Wang H, Nie J, Qin Z, Li J, Xiao W (2017) Analyte-triggered autocatalytic amplification combined with gold nanoparticle probes for colorimetric detection of heavy-metal ions. Chem Commun 53(54):7477–7480. https://doi.org/10.1039/C7CC02198D

21. Li Y, Si Y, Wang X, Ding B, Sun G, Zheng G, Luo W, Yu J (2013) Colorimetric sensor strips for lead (II) assay utilizing nanogold probes immobilized polyamide-6/nitrocellulose nano-fibers/nets. Biosens Bioelectron 48:244–250. https://doi.org/10.1016/j.bios.2013.03.085

22. Li Y, Ding B, Sun G, Ke T, Chen J, Al-Deyab SS, Yu J (2014) Solid-phase pink-to-purple chromatic strips utilizing gold probes and nanofibrous membranes combined system for lead (II) assaying. Sensors Actuators B Chem 204:673–681. https://doi.org/10.1016/j.snb.2014.08.048

23. Huang X, Jiang H, Li Y, Sang L, Zhou H, Shahzad SA, Ibupoto ZH, Yu C (2017) Synthesis of silica nanoparticles doped with [Ru(bpy)3]2+ and decorated with silver nanoclusters for the ratiometric photoluminescent determination and intracellular imaging of cu(II) ions. Microchim Acta 184(7):2325–2331. https://doi.org/10.1007/s00604-017-2206-3

24. Chaiyo S, Siangproh W, Apilux A, Chailapakul O (2015) Highly selective and sensitive paper-based colorimetric sensor using thiosulfate catalytic etching of silver nanoplates for trace determination of copper ions. Anal Chim Acta 866:75–83. https://doi.org/10.1016/j.aca.2015.01.042

25. Li Y, Wang L, Wen Y, Ding B, Sun G, Ke T, Chen J, Yu J (2015) Constitution of a visual detection system for lead(ii) on polydiacetylene-glycine embedded nanofibrous membranes. J Mater Chem A 3(18):9722–9730. https://doi.org/10.1039/C5TA00608B

26. Ding B, Si Y, Wang X, Yu J, Feng L, Sun G (2011) Label-free ultrasensitive colorimetric detection of copper(ii) ions utilizing polyaniline/polyamide-6 nano-fiber/net sensor strips. J Mater Chem 21(35):13345–13353. https://doi.org/10.1039/C1JM11851J

27. Zhang C, Wan LY, Wu S, Wu D, Qin X, Ko F (2015) A reversible colorimetric chemosensor for naked-eye detection of copper ions using poly (aspartic acid) nanofibrous hydrogel. Dyes Pigments 123(supplement C):380–385. https://doi.org/10.1016/j.dyepig.2015.07.028

28. Wu W-C, Lai H-J (2016) Preparation of thermo-responsive electrospun nanofibers containing rhodamine-based fluorescent sensor for Cu2+ detection. J Polym Res 23(11):223. https://doi.org/10.1007/s10965-016-1115-1

29. Pakiari AH, Jamshidi Z (2007) Interaction of amino acids with gold and silver clusters. J Phys Chem A 111(20):4391–4396. https://doi.org/10.1021/jp070306t

30. Grosse AC, Dicinoski GW, Shaw MJ, Haddad PR (2003) Leaching and recovery of gold using ammoniacal thiosulfate leach liquors (a review). Hydrometallurgy 69(1):1–21. https://doi.org/10.1016/S0304-386X(02)00169-X

31. Lou T, Chen L, Chen Z, Wang Y, Chen L, Li J (2011) Colorimetric detection of trace copper ions based on catalytic leaching of silver-coated gold nanoparticles. ACS Appl Mater Interfaces 3(11):4215–4220. https://doi.org/10.1021/am2008486

32. Xu B, Yang Y, Li Q, Yin W, Jiang T, Li G (2016) Thiosulfate leaching of au, ag and Pd from a high Sn, Pb and Sb bearing decopperized anode slime. Hydrometallurgy 164:278–287. https://doi.org/10.1016/j.hydromet.2016.06.011

33. Amendola V, Meneghetti M (2009) Size evaluation of gold nanoparticles by UV−Vis spectroscopy. J Phys Chem C 113(11):4277–4285. https://doi.org/10.1021/jp8082425

34. Luo Z, Yuwen L, Han Y, Tian J, Zhu X, Weng L, Wang L (2012) Reduced graphene oxide/PAMAM–silver nanoparticles nanocomposite modified electrode for direct electrochemistry of glucose oxidase and glucose sensing. Biosens Bioelectron 36(1):179–185. https://doi.org/10.1016/j.bios.2012.04.009

35. Ma Y, Li W, Cho EC, Li Z, Yu T, Zeng J, Xie Z, Xia Y (2010) Au@ag Core−Shell Nanocubes with finely tuned and well-controlled sizes, Shell thicknesses, and optical properties. ACS Nano 4(11):6725–6734. https://doi.org/10.1021/nn102237c

36. Huang Z-M, Zhang YZ, Kotaki M, Ramakrishna S (2003) A review on polymer nanofibers by electrospinning and their applications in nanocomposites. Compos Sci Technol 63(15):2223–2253. https://doi.org/10.1016/S0266-3538(03)00178-7

37. Wang X, Fu Q, Wang X, Si Y, Yu J, Wang X, Ding B (2015) In situ cross-linked and highly carboxylated poly(vinyl alcohol) nanofibrous membranes for efficient adsorption of proteins. J Mater Chem B 3(36):7281–7290. https://doi.org/10.1039/C5TB01192B

38. Zhang Z, Li X, Wang C, Fu S, Liu Y, Shao C (2009) Polyacrylonitrile and carbon nanofibers with controllable Nanoporous structures by electrospinning. Macromol Mater Eng 294(10):673–678. https://doi.org/10.1002/mame.200900076

39. Neghlani PK, Rafizadeh M, Taromi FA (2011) Preparation of aminated-polyacrylonitrile nanofiber membranes for the adsorption of metal ions: comparison with microfibers. J Hazard Mater 186(1):182–189